JGR Solid Earth

RESEARCH ARTICLE
10.1029/2020JB021259

Seismic Anisotropy and Mantle Deformation Beneath the Central Sunda Plate

Wenkai Song[1], Youqiang Yu[1,2,3], Stephen S. Gao[2], Kelly H. Liu[2], and Yifang Fu[1]

[1]State Key Laboratory of Marine Geology, Tongji University, Shanghai, China, [2]Geology and Geophysics Program, Missouri University of Science and Technology, Rolla, MO, USA, [3]Shanghai Sheshan National Geophysical Observatory, Shanghai, China

Key Points:

- Complex mantle deformation is revealed under the central Sunda plate from systematic shear wave splitting analysis
- Subduction-dominated and regionally slab tear-induced flow systems exist beneath the Malay Peninsula
- Flow related to the absolute plate motion is observed in northern Borneo and is locally deflected by a fossil slab segment

Supporting Information:

- Supporting Information S1
- Table S1
- Table S2
- Table S3

Correspondence to:
Y. Yu,
yuyouqiang@tongji.edu.cn

Citation:
Song, W., Yu, Y., Gao, S. S., Liu, K. H., & Fu, Y. (2021). Seismic anisotropy and mantle deformation beneath the central Sunda plate. *Journal of Geophysical Research: Solid Earth*, *126*, e2020JB021259. https://doi.org/10.1029/2020JB021259

Received 26 OCT 2020
Accepted 8 FEB 2021

Abstract The central Sunda plate, which forms the core of Southeast Asia, has been extensively studied based on analyses of data mainly from surface geological observations. In contrast, largely due to the limited coverage by seismic stations in the area, a number of key issues associated with mantle structure and dynamics remain enigmatic. These can possibly be constrained by investigating seismic azimuthal anisotropy in the upper mantle. Here we employ the shear wave splitting technique on three P-to-S converted phases from the core-mantle boundary (PKS, SKKS, and SKS) recorded by 11 stations to systematically explore the spatial variation of azimuthal anisotropy beneath the central Sunda plate. Most of the Malay Peninsula is revealed to possess mostly trench-perpendicular fast orientations that can be attributed to mantle flow induced by the Indo-Australian subduction. In addition, the central part of the Malay Peninsula is characterized by a 2-layered model of anisotropy, which is possibly associated with the joint effects of lithospheric fabrics and a slab tear-induced toroidal flow. Absolute plate motion (APM)-parallel anisotropy is observed in northern Borneo and the Nansha Block, where APM-driven simple shear in the transitional layer between the partially coupled lithosphere and asthenosphere is mostly responsible for the observed anisotropy. The APM-induced flow may be locally modified by a fossil slab segment beneath Sabah.

1. Introduction

The Sunda plate (Figure 1), which was previously considered the southernmost portion of the Eurasian plate (Bird, 2003; Simons et al., 2007) and is surrounded by active subduction zones except for its northern margin, is characterized by its distinctive kinematics with regard to adjacent plates (Bird, 2003). The westward subduction of the Philippine Sea plate and the east- and northward subduction of the Indo-Australian plate beneath the Sunda plate promoted the development of some of the most active and complex tectonic settings in the world (Hall, 2002, 2017). Extensive geological observations have revealed that the central portion of the Sunda plate has also undergone remarkable Cenozoic deformation (Hall, 2017 and referenced therein). However, details on mantle deformation patterns and related dynamics remain inconclusive, despite some recent large-scale regional tomography studies (e.g., Hall & Spakman, 2015; Huang et al., 2015; Zenonos et al., 2019) that have provided a general picture of mantle structure anomalies. For instance, it is not well understood to what extent the current and past subductions, such as, the Proto-South China Sea subduction (e.g., Hall, 2002, 2012; Zahirovic et al., 2016), have affected the surrounding mantle, and whether the corresponding mantle kinematics bear resemblance to the surface deformation.

One approach to help further decipher mantle dynamic beneath the central Sunda plate is to measure upper mantle deformation via analysis of seismic azimuthal anisotropy. Shear wave splitting (SWS) analysis provides a direct and robust avenue to quantify seismic azimuthal anisotropy of the mantle (e.g., Savage, 1999; Silver, 1996). When a shear wave propagates through an anisotropic medium, it splits into two quasishear waves with different wave speeds and polarizations that are orthogonal to each other. The splitting parameters (including fast orientation and splitting delay time) could be employed to determine the orientation and intensity of anisotropy (Silver & Chan, 1991). The observed seismic anisotropy has been commonly interpreted as originating from preferred orientation of anisotropic minerals (primarily olivine) associated with lithospheric deformation or asthenospheric flow (Karato et al., 2008; Zhang & Karato, 1995).

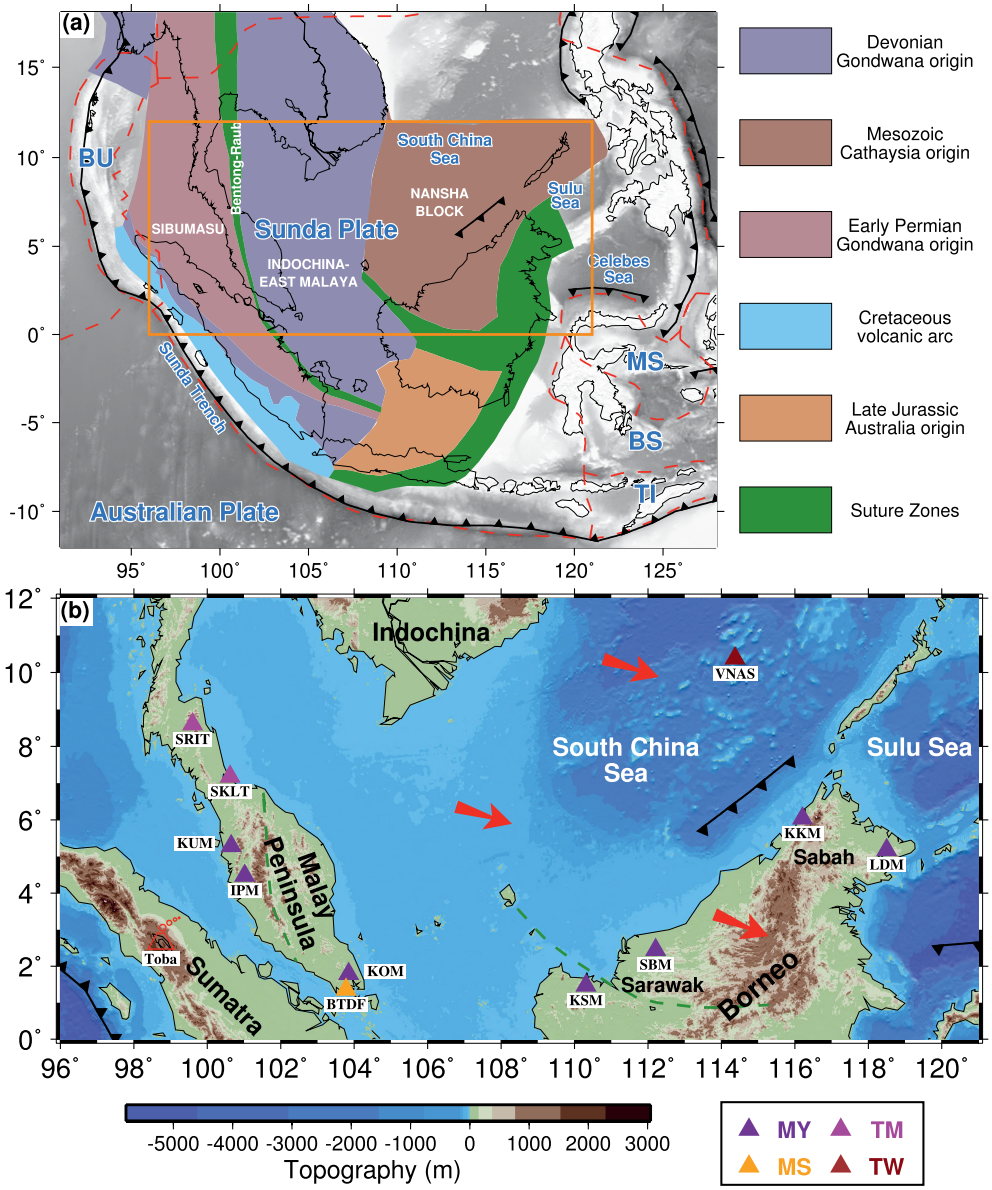

Figure 1. (a) Major geological terranes of the Sunda plate (modified after Hall, 2017; Hall & Sevastjanova, 2012). The orange rectangle depicts the study area in (b). Black solid and red dashed lines indicate trenches and plate boundaries, respectively. BS, Banda Sea; BU, Burma; MS, Molucca Sea; TI, Timor. (b) Topographic map of the study area showing seismic stations (triangles) used in the study. The triangle colors represent different seismic networks. The dashed green lines represent major sutures (Hutchison, 1975). The red arrows delineate the current absolute plate motion (APM) directions of the Sunda plate according to the NNR-MORVEL56 (Argus et al., 2011).

Several seismic anisotropy investigations have been conducted in the central Sunda Plate and surrounding areas to explore the upper mantle seismic anisotropy and associated mantle deformation (Figure S1; Collings et al., 2013; Di Leo et al., 2012; Hammond et al., 2010; Kong, Gao, Liu, Zhang, et al., 2020; Wang & He, 2020; Xue et al., 2013; Y. Yu et al., 2018). While some SWS studies using local S and XKS (including SKS, SKKS, and PKS) waves suggested that the mantle wedge of the Sumatra subduction zone is generally isotropic (Hammond et al., 2010), trench-orthogonal azimuthal anisotropy has been observed and attributed to a corner flow system in the mantle wedge using data recorded by two temporary seismic networks (Collings et al., 2013). Recent azimuthal anisotropy observations using SWS and receiver functions also revealed observable anisotropy in the mantle wedge and beneath the slab, and proposed an escaping mantle

flow from the slab window beneath northern Sumatra (Kong, Gao, Liu, Zhang, et al., 2020). Three different shear phases (local S, SKS, and downgoing S) recorded in Indonesia were employed to investigate seismic anisotropy (Di Leo et al., 2012), and coast-parallel fast orientations were observed from four stations at southern Borneo, which was explained as fossil anisotropy in response to block rotation. Though a SWS study has been conducted in areas surrounding the South China Sea (Xue et al., 2013), the measurements are quite limited with only two SWS observations available at Borneo. Mantle flow dominantly driven by the rollback of the subducted Indian slab was proposed to interpret the pervasively E-W fast orientations beneath the Indochina Peninsula (Y. Yu et al., 2018). A source-side sS splitting analysis recently revealed the existence of simple 2-D corner flow in the Java and Philippine subduction zones (Wang & He, 2020). Thus, the spatial variation of mantle anisotropy and inferred mantle deformation beneath the central Sunda plate are still poorly constrained.

In this study, using broadband seismic data from 11 permanent stations with an average recoding time of 15 years distributed at the Malay Peninsula, Borneo and the Nansha Block, we use three core-refracted shear-wave phases (PKS, SKKS, and SKS) to systematically investigate seismic anisotropy beneath the central Sunda plate, for the purpose of improving our understanding on its mantle deformation and dynamic processes.

2. Tectonic Setting

The central Sunda plate is an assemblage of various terranes derived from allochthonous continental fragments at different geological times (Figure 1a; Hall, 2017; Hall & Sevastjanova, 2012). It mainly comprises parts of the Sibumasu terrane, Indochina-East Malaya area, Borneo and the Nansha Block (Figure 1). The Sibumasu terrane, which separated from NW Australian Gondwana in the Early Permian, moved northwards and collided in the Triassic with the Indochina-East Malaya area that originated from Gondwana in the Devonian (Figure 1), forming the orogenic Bentong-Raub suture zone in between (Hall, 2017; Hall & Sevastjanova, 2012; Metcalfe, 2000, 2013). The Bentong-Raub suture is believed to signify the remnant of the Paleo-Tethys ocean subduction beneath the Indochina-East Malaya terrane, which was terminated in the late Middle Triassic (Metcalfe, 2000, 2013). Such an orogenic event led to crustal thickening beneath the Sibumasu terrane in the Triassic with a thickness of about 43 km (Ghani et al., 2013; Metcalfe, 2000), which was recently revealed to be thinned to around 30 km associated with the Late Paleogene rifting and a subsequent thermal anomaly (J. Gao et al., 2020).

Situated at approximately the center of the Sunda plate, Borneo, the third-largest island in the world, is recognized to stem from the amalgamation of multiple plate fragments (Figure 1a; Hall, 2017; Hall & Sevastjanova, 2012). Cenozoic tectonic evolution of northern Borneo highly correlates with the southward subduction of the hypothetical Proto-South China Sea starting in the Paleogene (e.g., Hall, 2002, 2012; Zahirovic et al., 2016). The Proto-South China Sea was entirely consumed in the Early Miocene when the Nansha Block collided with northern Borneo, giving rise to slab breakoff and subsequent orogenesis at northern Borneo (Hall, 2002; Zahirovic et al., 2016). Tomographic studies revealed a high-velocity anomaly situated in the upper mantle beneath NE Borneo, which was interpreted as the remnant slab segment of the Proto-South China Sea (Tang & Zheng, 2013; Zenonos et al., 2019).

The continuous subduction of the Indo-Australian plate makes Sumatra a tectonically active area. Part of the subducted slab was imaged to have reached the mantle transition zone beneath the Malay Peninsula (e.g., Hall & Spakman, 2015; Huang et al., 2015; Kong, Gao, Liu, Ding, et al., 2020; S. Liu, Suardi, et al., 2019) and under the Burma arc, forming a big mantle wedge (Lei & Zhao, 2016; Lei et al., 2009, 2019). Plate reconstructions (e.g., Hall, 2012; Whittaker et al., 2007; Zahirovic et al., 2016) indicated that significant rollback of the subducted Indo-Australian plate can plausibly account for the prevalent extension within the western Sunda plate from Eocene to Miocene (Morley, 2001; Pubellier & Morley, 2014). A slab tear was revealed to exist beneath northern Sumatra (e.g., Hall & Spakman, 2015; S. Liu, Suardi, et al., 2019; Zenonos et al., 2019) and offered a pathway for subslab materials to travel through it into the mantle wedge (Kong, Gao, Liu, Zhang, et al., 2020).

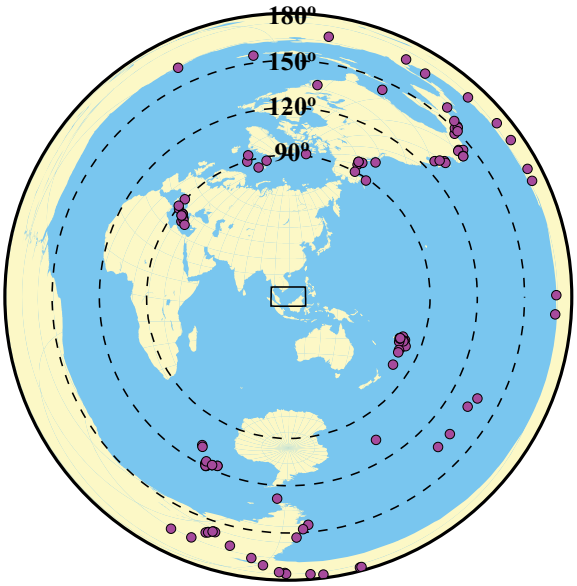

Figure 2. Distributions of events (magenta dots) used in the study. The rectangle indicates the study area. Note that the minimum epicentral distances are 120°, 95°, and 84° for PKS, SKKS, and SKS, respectively.

3. Data and Methods

We utilized broadband seismic data recorded over the period of 1999–2019 by 11 permanent stations (Figure 1b), among which 7 stations belong to the Malaysian National Seismic Network (network code: MY), two stations at the northern Malay Peninsula are operated by the Thai Seismic Monitoring Network (network code: TM), one station belongs to the Singapore Seismological Network (network code: MS), and one station on the Taiping Island (also called Itu Aba Island) of the Nansha Block is part of the Broadband Array in Taiwan for Seismology (network code: TW). All the data were requested from the Incorporated Research Institutions for Seismology (IRIS) Data Management Center (DMC) and are publicly accessible.

The epicentral distance ranges used for data request are 120°–180°, 95°–180°, and 84°–180° for PKS, SKKS, and SKS, respectively (Figure 2), with the cutoff magnitude of 5.6 for focal depths less than 100 km and 5.5 for focal depths larger than 100 km (K. H. Liu & Gao, 2013). The raw waveforms were bandpass filtered using a four-pole two-pass Butterworth filter with a corner frequency between 0.04 and 0.5 Hz. We then applied the SWS measuring and ranking procedures developed by K. H. Liu et al. (2008), which incorporate the transverse component energy minimization method (Silver & Chan, 1991), to process the filtered waveforms and obtain initial SWS results. It is noteworthy that a 17° of sensor misorientation has been corrected for station SRIT (Y. Yu, Hung, et al., 2017) after which the SWS measurements have been significantly improved (Y. Yu et al., 2018).

The resulting SWS waveforms were visually inspected and ranked following the criteria of K. H. Liu and Gao (2013) in terms of the quality of XKS arrivals and the corresponding particle motions. Retained splitting results possess high signal-to-noise ratio XKS arrivals on both the original radial and transverse components but significantly reduced XKS signal on the corrected transverse component, high similarity between the fast and slow shear-wave waveforms, and elliptical original and linear corrected particle motions (Figure 3). In addition, we have also identified null measurements, which are characterized as prominent XKS energy on the original radial while no identifiable energy on the original transverse components. Examples of well-defined and null measurements are shown in Figure 3 and Figure S2, respectively (similar plots for all the measurements can be accessed at http://web.mst.edu/%7Eyyqkc/Proj/20a-sunda-sws).

4. Results

There is a total of 130 well-defined XKS measurements obtained from 108 events (Figure 2) including 20 PKS, 52 SKKS, and 58 SKS (Figure 4), and 31 null measurements (Figure S3). The resulting fast orientations range from 7.0° to 146.0° with a circular mean of 83.6° ± 35.2°, and the observed delay times vary from 0.45 to 2.35 s with an average of 1.10 ± 0.44 s. Such a relatively broad range of delay times may be associated with laterally heterogeneous distributions of anisotropy strength (Figure S4) or the presence of complex anisotropy that induces the back azimuth (BAZ)-varying splitting parameters (Silver & Savage, 1994). Most of the resulting SWS measurements at each station are azimuthally independent (Figure S5) except for stations IPM and KUM (Figure 5), suggesting that simple anisotropy pervades beneath most of the study area. Our results are generally in line with those from previous studies at the Malay Peninsula (Di Leo et al., 2012; Y. Yu et al., 2018) and northern Borneo (Xue et al., 2013). However, Di Leo et al. (2012) and Xue et al. (2013) reported large delay times (greater than 2.5 s) in southern Malay Peninsula and Sabah, respectively, which are not revealed from our observations.

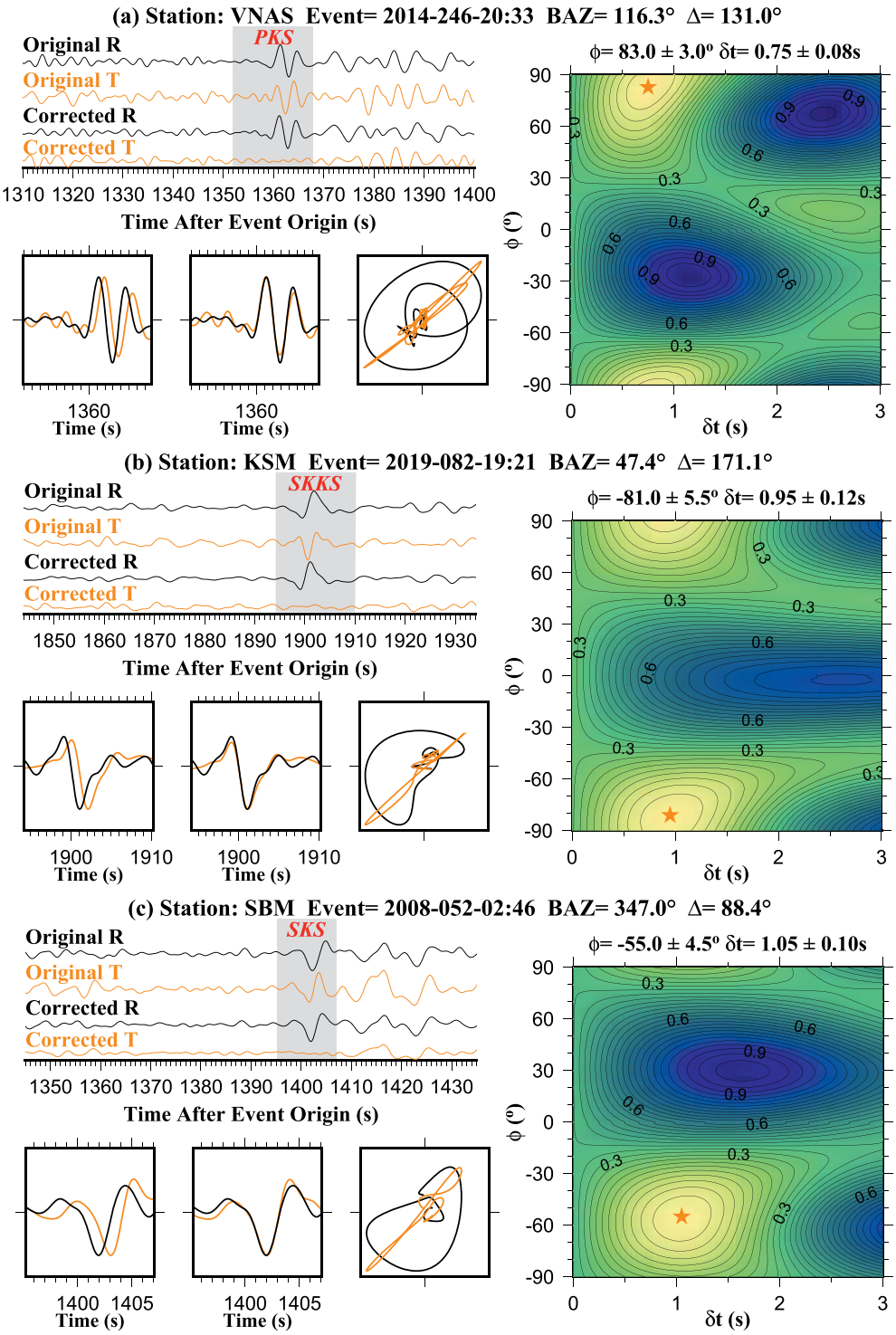

Figure 3. Examples of splitting measurements for (a) PKS, (b) SKKS, and (c) SKS phases. For each plot, the four waveforms on the top-left corner show the original radial, original transverse, corrected radial, and corrected transverse components, respectively. The XKS arrival is within the gray shaded window. The three panels beneath the four waveforms portray the original, and shifted fast (black) and slow (orange) waveforms, and original (black) and corrected (orange) particle motions, respectively. The contour map on the right displays the normalized energy of the corrected transverse components with the orange star representing the optimal splitting parameters. BAZ, back azimuth.

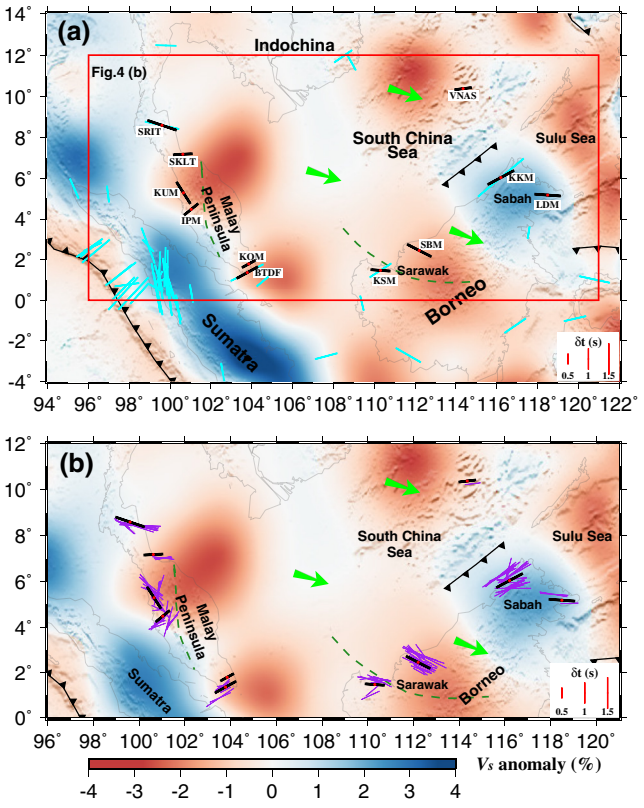

Figure 4. (a) Compilation of station-averaged XKS splitting measurements from this (black bars) and previous (cyan bars, e.g., Collings et al., 2013; Di Leo et al., 2012; Hammond et al., 2010; Kong, Gao, Liu, Zhang, et al., 2020; Xue et al., 2013; Y. Yu et al., 2018) studies. Red dots denote the station locations. The background image shows shear-wave velocity anomalies at 200 km depth from the tomography study of Zenonos et al. (2019). (b) Station-averaged (black bars) and individual (purple bars) shear wave splitting measurements plotted above the ray-piercing points at the depth of 200 km.

4.1. Malay Peninsula

A total of 59 observations were obtained from six stations at the Malay Peninsula, which show spatially varying splitting parameters. The fast orientations and delay times range from 7.0° to 146.0° and from 0.45 to 2.00 s, respectively, with corresponding mean values of 76.9° ± 42.0° and 0.98 ± 0.43 s. Most of the resulting fast orientations are perpendicular to the Sunda trench (Figure 4). A clear transition of the fast orientations exists near stations KUM and IPM where they gradually change from roughly NW-SE (133.1° ± 36.7°) in the northern area to generally NE-SW (49.1° ± 19.2°) in the southern area, respectively (Figure 4). In addition, azimuthal variations of the splitting parameters are observed at stations KUM and IPM (Figure 5), which are possibly suggestive of complex anisotropy (Silver & Savage, 1994).

4.2. Northern Borneo

The resultant SWS parameters at northern Borneo have an average fast orientation of 86.2° ± 28.7° and a mean delay time of 1.22 ± 0.41 s based on a total of 70 observations from four stations. Dominant NE-SW fast orientations (61.6° ± 15.3°) are locally revealed at station KKM near the Sabah area, which are in contrast with the generally SE-NW fast orientations at the other three stations (Figure 4). When results from station KKM are excluded, the mean delay time is calculated to be 1.10 ± 0.40 s and the average fast orientation is 108.2° ± 17.5°, which agrees well with the present absolute plate motion (APM) direction (about 110°) of Borneo based on the NNR-MORVEL56 model (Argus et al., 2011).

4.3. Nansha Block

There is only one station (VNAS) with data available in the Nansha Block and it is situated at the Taiping Island, the largest natural island of the Nansha Block. To our knowledge, it is the first time when data from station VNAS are employed for SWS analysis. Possibly due to the high background noise level, only one well-defined SWS measurement was obtained with a fast orientation of 83.0° ± 3.0° and a delay time of 0.75 ± 0.08 s. This is smaller than the mean delay time of the whole study area.

5. Discussion

5.1. Analysis of Anisotropy Depths

Most of the resulting fast orientations are oblique or even orthogonal to the strikes of the lithospheric fabrics especially those at the Malay Peninsula (Figure 4). In addition, if we assume a typical anisotropic strength of 4% (Savage, 1999) and a mean lithospheric shear wave velocity of 4.41 km/s (Tang & Zheng, 2013), the observed average delay time of 1.10 s requires a lithospheric thickness of at least 120 km beneath the study area, which is much thicker than what has been revealed from multifarious investigations, i.e., a range of 65–100 km (e.g., Shi et al., 2017; Tang & Zheng, 2013; C. Yu, Shi, et al., 2017). Thus, a lithospheric origin alone can hardly account for the observed seismic anisotropy of the study area, and contributions from the asthenosphere may play a significant role.

The resulting SWS measurements at each station mostly display an absence of azimuth variation (Figure S5) and may be explained by a single-layer anisotropy in the upper mantle (K. H. Liu & Gao, 2013; Silver & Savage, 1994). The main source of anisotropy is concluded to be within the upper mantle (Savage, 1999) and experimental studies (Karato, 1992) indicated that diffusion creep tends to dominate in the deeper

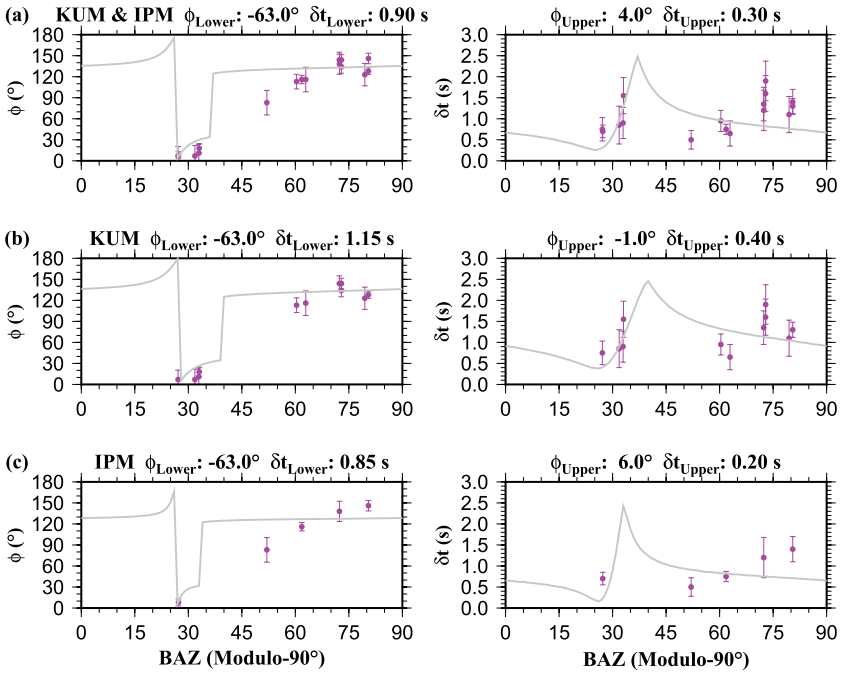

Figure 5. Azimuthal variations of observed (magenta dots) and theoretical (gray lines) splitting parameters computed using parameters of a two-layered model above the panels. (a) The optimal fitting results based on combined measurements from stations KUM and IPM. (b) Same as (a) but using observations from station KUM. (c) Same as (b) but for station IPM. Note that measurements from station IPM employed in the two-layered anisotropic analysis are only within the BAZ range of 270°–90° (270°–360° and 0°–90°).

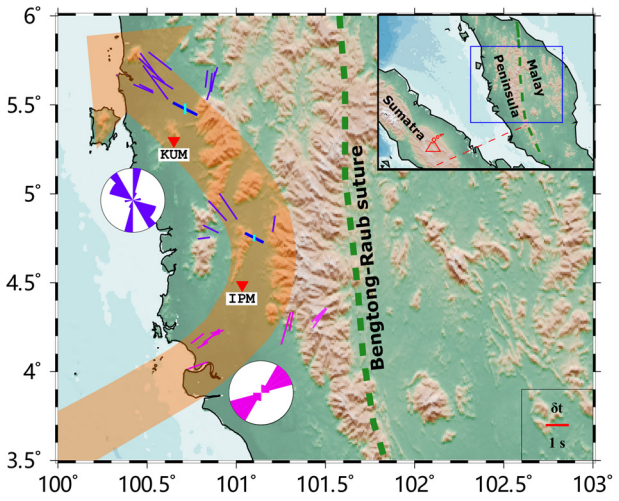

Figure 6. Individual splitting parameters for stations IPM and KUM plotted above the ray-piercing points at the depth of 200 km (magenta and violet bars). The blue and cyan bars represent splitting parameters for the lower- and upper-layer anisotropy of each station, respectively. The magenta and violet bars correspond to individual splitting parameters within the BAZ ranges of 90°–270° and 270°–90°. The rose diagram portrays the fast orientations from each corresponding BAZ range. The shaded orange arrow indicates the toroidal flow. The inset map manifests the location of two stations with respect to Sumatra. The dashed red line approximately indicates the middle position of slab tear based on tomography images (S. Liu, Suardi, et al., 2019).

upper mantle, leading to an isotropic structure. Body-wave anisotropy tomography in SE Asia also revealed that strong anisotropy mostly exists in the upper mantle (Huang et al., 2015). The azimuth-dependent measurements within the BAZ range of 270°–90° (0°–90° and 270°–360°) observed at stations KUM and IPM possess a prominent 90° periodicity (Figure 5), which may be indicative of complex anisotropy (K. H. Liu & Gao, 2013; Silver & Savage, 1994). In comparison, the remaining SWS measurements within the BAZ range of 90°–270° from station IPM display a different pattern and rarely change with respect to the BAZ (Figure 6).

5.2. Characteristics of the Mantle Flow Field Beneath the Malay Peninsula

Although our results combined with previous observations (Di Leo et al., 2012; Y. Yu et al., 2018) manifest that the fast orientations change from nearly E-W in the northern to NE-SW in the southern Malay Peninsula, most of them are perpendicular to the trench axis (Figure 4 and Figure S1). These trench-perpendicular fast orientations possibly result from mantle flow associated with the Indo-Australian subduction as imaged by tomography studies (Hall & Spakman, 2015; Huang et al., 2015; S. Liu, Suardi, et al., 2019; Zenonos et al., 2019). A global compilation of SWS measurements in the subduction zones (Long, 2013) concluded that most of the fast orientations orthogonal to the trench strike can be attributed to a trench-perpendicular mantle flow beneath the backarc regions, which is usually linked to either the corner flow (Long, 2013; Long & Silver, 2008) or slab rollback (Chen et al., 2016). A trench-perpendicular corner flow is usually driven by viscous coupling between the downgoing

slab and the overlying mantle (Long & Silver, 2008), which is widely revealed beneath active subductions of Tonga (Fischer et al., 2000) and western Pacific beneath Japan (X. Liu & Zhao, 2016). In comparison, slab rollback would generate a trench-normal horizontal velocity gradient under the overriding plate and further induce a basal drag force, which can also develop trench-perpendicular mantle flow and drive backarc extension (Chen et al., 2016). Extensions surrounding the Malay Peninsula have been commonly interpreted as the consequence of slab rollback in response to the Indo-Australian subduction based on evidences from geological observations (Morley, 2001; Pubellier & Morley, 2014), plate reconstructions (Whittaker et al., 2007; Zahirovic et al., 2016) and physical modeling (Schellart & Lister, 2005). Slab rollback-induced mantle flow is also proposed to be responsible for the E-W fast orientations observed at the Indochina Peninsula (Y. Yu et al., 2018).

Complex anisotropy revealed at stations KUM and IPM in the middle of the Malay Peninsula can be constrained by incorporating a two-layered anisotropic modeling procedure (Silver & Savage, 1994), which employs a weighted misfit function to grid search for the optimal splitting parameters for an assumed two-layered anisotropy model (S. S. Gao & Liu, 2009). The weighting factors were assigned as 0.8 for fast orientations and 0.2 for delay times by considering the strength of variation patterns for each of the splitting parameters (Figure 5). Following a two-step approach previously employed in the Tian Shan (Cherie et al., 2016) and Malawi rift (Reed et al., 2017), we first combined measurements within the BAZ range of 270°–90° (270°–360° and 0°–90°) from these two stations (stations KUM and IPM) and then determined the two pairs of splitting parameters, which are calculated to be (−63°, 0.90 s) for the lower layer and (4°, 0.30 s) for the upper layer (Figure 5). We subsequently constrained the searching ranges of the fast orientations for each of the two stations by allowing a 30° perturbation from the above fast orientations. The resulting splitting measurements of the upper layers for stations KUM (−1°, 0.40 s) and IPM (6°, 0.20 s) are similar, with their fast orientations generally parallel to the strike of the orogenic Bentong-Raub suture (Figure 6). The delay times are comparable to the typical magnitude of crustal anisotropy (Savage, 1999). The development of the orogenic Bentong-Raub suture would promote vertically coherent deformation and generate fossil anisotropy in the crust/lithosphere (Silver, 1996), which may offer a viable explanation for the revealed upper-layer anisotropy.

The resulting fast orientations of the lower layer for either station KUM or IPM are identical to the one (−63°) from analysis of the combined measurements, which is oblique to the trench axis. When considering the SWS measurements from station IPM within the BAZ of 90°–270° and the lower layer of both stations KUM and IPM, the fast orientations generally depict a pattern of rotation (Figure 6). Both local and regional tomography studies (Hall & Spakman, 2015; S. Liu, Suardi, et al., 2019; Zenonos et al., 2019) revealed a slab tear beneath northern Sumatra (Figures 6 and 7), which is prone to instigate a toroidal flow at the slab edge (Chen et al., 2016; Long, 2013; Long & Silver, 2008). The existence of such a flow system was further suggested by a recent SWS investigation in the Sumatra area (Kong, Gao, Liu, Zhang, et al., 2020) where the fast orientations changed from trench-perpendicular in the forearc area to trench-parallel in the backarc region. Thus, the lower-layer anisotropy revealed beneath the central Malay Peninsula can possibly be attributed to the toroidal flow induced by the tear of the subducted Indo-Australian slab. A similar model associated with the Indian slab tear (L. Liu, Gao, et al., 2019) and the big mantle wedge (Lei & Zhao, 2016; Lei et al., 2009, 2019) is also proposed to explain the circular fast orientations observed in the eastern Himalayan syntaxis and the trench-perpendicular fast orientations in the eastern Tibet toward the Burma arc. The revealed two-layered anisotropy is also consistent with that from 3D body-wave anisotropy tomography (Huang et al., 2015). We suggest that mantle flow induced by the Indo-Australian subduction is the major cause for the observed dominantly trench-perpendicular fast orientations observed beneath the Malay Peninsula. Slab tear-induced mantle flow and fossil anisotropy contribute to the regionally deciphered complex anisotropy beneath the central Malay Peninsula.

5.3. APM-Induced Anisotropy and Partially Deflected Flow

The vast majority of the resulting fast orientations observed at northern Borneo (except those from station KKM at Sabah) and the Nansha Block (Figure 4) are spatially consistent with the APM directions predicted by the no-net rotation model of the NNR-MORVEL56 (Argus et al., 2011). Simple shear, as revealed by experimental studies, would orient the crystallographic axes of anisotropic minerals toward the mantle flow

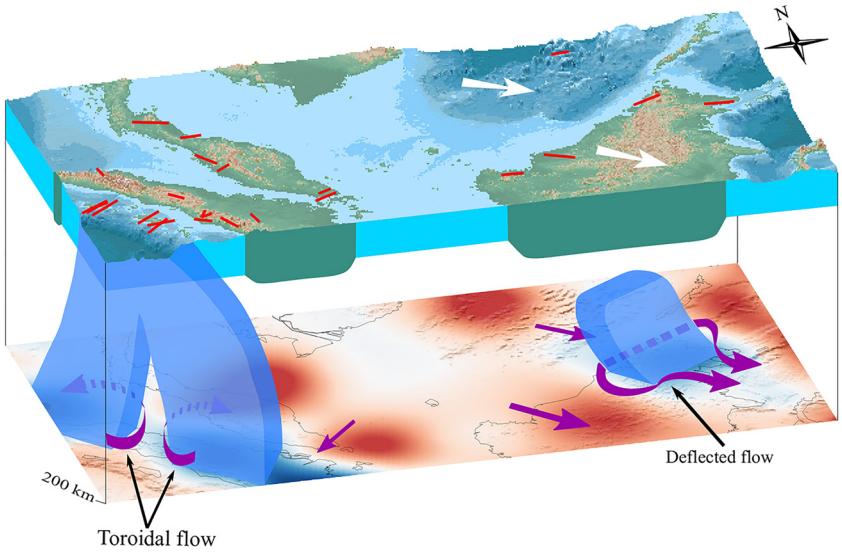

Figure 7. Schematic 3D model illustrating complex mantle flow systems that are responsible for the observed splitting parameters. The mantle flow directions are highlighted by the dark violet arrows. Red bars represent splitting measurements from this and previous (Kong, Gao, Liu, Zhang, et al., 2020) studies. White arrows denote the APM directions. Note that there is an approximately four time vertical exaggeration for clarity.

direction in the asthenosphere (Karato et al., 2008; Zhang & Karato, 1995), and APM-parallel azimuthal anisotropy can be formed by the relative movement between the overriding lithosphere and the underlying asthenosphere (Conrad & Behn, 2010; Silver, 1996). Such APM-parallel anisotropy may be indicative of significant lithosphere-asthenosphere coupling and can be driven by a certain degree of viscosity difference at the base of the lithosphere (Marone & Romanowicz, 2007). The viscosity contrast between the lithosphere and asthenosphere obtained from inversion of shear wave velocity structure (C. Yu, Shi, et al., 2017) was revealed to be significantly lower than what is required for the occurrence of decoupling according to numerical modeling studies (Doglioni et al., 2011). Surface wave investigations (Tang & Zheng, 2013) indicated that there is a low velocity layer with approximately 100 km thickness underlying the base of the lithosphere beneath northern Borneo and the Nansha Block, possibly representing the gradual transitional layer from the lithosphere to the asthenosphere, which can well account for the observed average 1.10 s splitting time with an assumed mean anisotropy of 4% (Savage, 1999). Thus, most of the observed APM-parallel anisotropy can possibly be attributed to the simple shear in the upper asthenosphere associated with the relative movement and partial coupling between the lithosphere and asthenosphere (Figure 7). This mechanism is also consistent with the modeled mantle flow field of the eastern Sunda plate by taking into account the current APM and upper mantle viscosity structure (Conrad & Behn, 2010).

A conspicuous exception (station KKM) that contradicts the APM-induced mantle flow model is situated at Sabah, where the resultant fast orientations (61.6° ± 15.3°) are significantly oblique to the APM direction (Figure 4). Such a discrepancy is possibly indicative of a localized mantle flow field. Both surface- (Tang & Zheng, 2013) and body-wave (Zenonos et al., 2019) tomography studies have imaged a high-velocity anomaly residing in the sublithospheric mantle (about 100–300 km) beneath Sabah, which has been interpreted as fossil slab segment inherited from the southward Proto-South China Sea subduction. The existence of the rigid slab segment or thick lithospheric keel could deflect the APM-induced NW-SE mantle flow to travel along the edges, leading to the observed NE-SW fast orientations (Figure 7). Such a deflected flow system has been widely employed to explain SWS measurements along the edges of regions with thick lithospheric roots such as the North American continent (Fouch et al., 2000; Refayee et al., 2014; Yang et al., 2017), the Great Xing'an range in NE China (Lu et al., 2020), cratons in southern Africa (Reed et al., 2017; Y. Yu et al., 2015) and continental keels beneath the South Carpathians (Song et al., 2019).

6. Conclusions

In this study, we have revealed systematic spatial variations of seismic azimuthal anisotropy beneath the central Sunda plate based on data recorded by 11 broadband seismic stations at the Malay Peninsula, northern Borneo, and the Nansha Block. Most of the resulting fast orientations at the Malay Peninsula are perpendicular to the trench strike, and may result from a trench-normal mantle flow induced by the Indo-Australian subduction. However, complex anisotropy is locally revealed in the central Malay Peninsula where the upper-layer anisotropy may have a lithospheric origin associated with the fossil orogenic sutures, and the lower-layer anisotropy is attributable to a slab tear-induced toroidal flow. In comparison, the vast majority of the observed fast orientations in northern Borneo and the Nansha Block are NW-SE and are consistent with the APM directions, which can be best explained by the shear strain within the rheologically transitional layer between the lithosphere and asthenosphere. Such an APM-induced flow may be locally modified by the horizontal deflection of the slab segments inherited from the Proto-South China Sea subduction.

Data Availability Statement

All seismic data used in this study can be freely accessed from the Incorporated Research Institutions for Seismology (IRIS) Data Management Center (https://ds.iris.edu/ds/nodes/dmc). Figures were made using the Generic Mapping Tools (Wessel & Smith, 1998) and Inkscape (https://inkscape.org).

Acknowledgments
This study is funded by the National Program on Global Change and Air-Sea Interaction (grant GASIGEOGE-05) and the National Natural Science Foundation of China (grant 42074052), and Shanghai Sheshan National Geophysical Observatory (grant 2020K04). The authors thank Aristides Zenonos for kindly providing his tomographic results. Constructive comments from James Hammond and an anonymous reviewer greatly improved the manuscript.

References

Argus, D. F., Gordon, R. G., & DeMets, C. (2011). Geologically current motion of 56 plates relative to the no-net-rotation reference frame. *Geochemistry, Geophysics, Geosystems*, *12*, Q11001. https://doi.org/10.1029/2011GC003751

Bird, P. (2003). An updated digital model of plate boundaries. *Geochemistry, Geophysics, Geosystems*, *4*, 1027. https://doi.org/10.1029/2001GC000252

Chen, Z., Schellart, W. P., Strak, V., & Duarte, J. C. (2016). Does subduction-induced mantle flow drive backarc extension? *Earth and Planetary Science Letters*, *441*, 200–210. https://doi.org/10.1016/j.epsl.2016.02.027

Cherie, S. G., Gao, S. S., Liu, K. H., Elsheikh, A. A., Kong, F., Reed, C. A., & Yang, B. B. (2016). Shear wave splitting analyses in Tian Shan: Geodynamic implications of complex seismic anisotropy. *Geochemistry, Geophysics, Geosystems*, *17*, 1975–1989. https://doi.org/10.1002/2016GC006269

Collings, R., Rietbrock, A., Lange, D., Tilmann, F., Nippress, S., & Natawidjaja, D. (2013). Seismic anisotropy in the Sumatra subduction zone. *Journal of Geophysical Research: Solid Earth*, *118*, 5372–5390. https://doi.org/10.1002/jgrb.50157

Conrad, C. P., & Behn, M. D. (2010). Constraints on lithosphere net rotation and asthenospheric viscosity from global mantle flow models and seismic anisotropy. *Geochemistry, Geophysics, Geosystems*, *11*, Q05W05. https://doi.org/10.1029/2009GC002970

Di Leo, J. F., Wookey, J., Hammond, J. O. S., Kendall, J.-M., Kaneshima, S., Inoue, H., et al. (2012). Mantle flow in regions of complex tectonics: Insights from Indonesia. *Geochemistry, Geophysics, Geosystems*, *13*, Q12008. https://doi.org/10.1029/2012GC004417

Doglioni, C., Ismail-Zadeh, A., Panza, G., & Riguzzi, F. (2011). Lithosphere–asthenosphere viscosity contrast and decoupling. *Physics of the Earth and Planetary Interiors*, *189*, 1–8. https://doi.org/10.1016/j.pepi.2011.09.006

Fischer, K. M., Parmentier, E. M., Stine, A. R., & Wolf, E. R. (2000). Modeling anisotropy and plate-driven flow in the Tonga subduction zone back arc. *Journal of Geophysical Research*, *105*, 16181–16191. https://doi.org/10.1029/1999JB900441

Fouch, M. J., Fischer, K. M., Parmentier, E. M., Wysession, M. E., & Clarke, T. J. (2000). Shear-wave splitting, continental keels, and patterns of mantle flow. *Journal of Geophysical Research*, *105*, 6255–6275. https://doi.org/10.1029/1999JB900372

Gao, J., Yu, Y., Song, W., Gao, S. S., & Liu, K. H. (2020). Crustal modifications beneath the central Sunda plate associated with the Indo-Australian subduction and the evolution of the South China Sea. *Physics of the Earth and Planetary Interiors*, *306*, 106539. https://doi.org/10.1016/j.pepi.2020.106539

Gao, S. S., & Liu, K. H. (2009). Significant seismic anisotropy beneath the southern Lhasa Terrane, Tibetan Plateau. *Geochemistry, Geophysics, Geosystems*, *10*, Q02008. https://doi.org/10.1029/2008GC002227

Ghani, A. A., Lo, C.-H., & Chung, S.-L. (2013). Basaltic dykes of the Eastern Belt of Peninsular Malaysia: The effects of the difference in crustal thickness of Sibumasu and Indochina. *Journal of Asian Earth Sciences*, *77*, 127–139. https://doi.org/10.1016/j.jseaes.2013.08.004

Hall, R. (2002). Cenozoic geological and plate tectonic evolution of SE Asia and the SW Pacific: Computer-based reconstructions, model and animations. *Journal of Asian Earth Sciences*, *20*, 353–431. https://doi.org/10.1016/S1367-9120(01)00069-4

Hall, R. (2012). Late Jurassic–Cenozoic reconstructions of the Indonesian region and the Indian Ocean. *Tectonophysics*, *570–571*, 1–41. https://doi.org/10.1016/j.tecto.2012.04.021

Hall, R. (2017). Southeast Asia: New views of the geology of the Malay Archipelago. *Annual Review of Earth and Planetary Sciences*, *45*, 331–358. https://doi.org/10.1146/annurev-earth-063016-020633

Hall, R., & Sevastjanova, I. (2012). Australian crust in Indonesia. *Australian Journal of Earth Sciences*, *59*, 827–844. https://doi.org/10.1080/08120099.2012.692335

Hall, R., & Spakman, W. (2015). Mantle structure and tectonic history of SE Asian. *Tectonophysics*, *658*, 14–45. https://doi.org/10.1016/j.tecto.2015.07.003

Hammond, J. O. S., Wookey, J., Kaneshima, S., Inoue, H., Yamashina, T., & Harjadi, P. (2010). Systematic variation in anisotropy beneath the mantle wedge in the Java–Sumatra subduction system from shear-wave splitting. *Physics of the Earth and Planetary Interiors*, *178*, 189–201. https://doi.org/10.1016/j.pepi.2009.10.003

Huang, Z., Zhao, D., & Wang, L. (2015). P wave tomography and anisotropy beneath Southeast Asia: Insight into mantle dynamics. *Journal of Geophysical Research: Solid Earth*, *120*, 5154–5174. https://doi.org/10.1002/2015JB012098

Hutchison, C. S. (1975). Ophiolite in Southeast Asia. *Geological Society of America Bulletin*, *86*, 797–806. https://doi.org/10.1130/0016-7606(1975)86<797:OISA>2.0.CO;2

Karato, S. (1992). On the Lehmann discontinuity. *Geophysical Research Letters*, *19*, 2255–2258. https://doi.org/10.1029/92GL02603

Karato, S., Jung, H., Katayama, I., & Skemer, P. (2008). Geodynamic significance of seismic anisotropy of the upper mantle: New insights from laboratory studies. *Annual Review of Earth and Planetary Sciences*, *36*, 59–95. https://doi.org/10.1146/annurev.earth.36.031207.124120

Kong, F., Gao, S. S., Liu, K. H., Ding, W., & Li, J. (2020). Slab dehydration and mantle upwelling in the vicinity of the Sumatra subduction zone: Evidence from receiver function imaging of mantle transition zone discontinuities. *Journal of Geophysical Research: Solid Earth*, *125*, e2020JB019381. https://doi.org/10.1029/2020JB019381

Kong, F., Gao, S. S., Liu, K. H., Zhang, J., & Li, J. (2020). Seismic anisotropy and mantle flow in the Sumatra subduction zone constrained by shear wave splitting and receiver function analyses. *Geochemistry, Geophysics, Geosystems*, *21*, e2019GC008766. https://doi.org/10.1029/2019GC008766

Lei, J., & Zhao, D. (2016). Teleseismic P-wave tomography and mantle dynamics beneath Eastern Tibet. *Geochemistry, Geophysics, Geosystems*, *17*, 1861–1884. https://doi.org/10.1002/2016GC006262

Lei, J., Zhao, D., & Su, Y. (2009). Insight into the origin of the Tengchong intraplate volcano and seismotectonics in southwest China from local and teleseismic data. *Journal of Geophysical Research*, *114*, B05302. https://doi.org/10.1029/2008JB005881

Lei, J., Zhao, D., Xu, X., Xu, Y.-G., & Du, M. (2019). Is there a big mantle wedge under eastern Tibet? *Physics of the Earth and Planetary Interiors*, *292*, 100–113. https://doi.org/10.1016/j.pepi.2019.04.005

Liu, K. H., & Gao, S. S. (2013). Making reliable shear-wave splitting measurements. *Bulletin of the Seismological Society of America*, *103*, 2680–2693. https://doi.org/10.1785/0120120355

Liu, K. H., Gao, S. S., Gao, Y., & Wu, J. (2008). Shear wave splitting and mantle flow associated with the deflected Pacific slab beneath northeast Asia. *Journal of Geophysical Research*, *113*, B01305. https://doi.org/10.1029/2007JB005178

Liu, L., Gao, S. S., Liu, K. H., Li, S., Tong, S., & Kong, F. (2019). Toroidal mantle flow induced by slab subduction and rollback beneath the Eastern Himalayan syntaxis and adjacent areas. *Geophysical Research Letters*, *46*, 11080–11090. https://doi.org/10.1029/2019GL084961

Liu, S., Suardi, I., Zheng, M., Yang, D., Huang, X., & Tong, P. (2019). Slab morphology beneath northern Sumatra revealed by regional and teleseismic traveltime tomography. *Journal of Geophysical Research: Solid Earth*, *124*, 10544–10564. https://doi.org/10.1029/2019JB017625

Liu, X., & Zhao, D. (2016). Backarc spreading and mantle wedge flow beneath the Japan Sea: Insight from Rayleigh-wave anisotropic tomography. *Geophysical Journal International*, *207*, 357–373. https://doi.org/10.1093/gji/ggw288

Long, M. D. (2013). Constraints on subduction geodynamics from seismic anisotropy. *Reviews of Geophysics*, *51*, 76–112. https://doi.org/10.1002/rog.20008

Long, M. D., & Silver, P. G. (2008). The subduction zone flow field from seismic anisotropy: A global review. *Science*, *319*, 315–318. https://doi.org/10.1126/science.1150809

Lu, M., Lei, J., Zhao, D., Ai, Y., Xu, X., & Zhang, G. (2020). SKS splitting measurements in NE China: New insights into the Wudalianchi intraplate volcanism and mantle dynamics. *Journal of Geophysical Research: Solid Earth*, *125*, e2019JB018575. https://doi.org/10.1029/2019JB018575

Marone, F., & Romanowicz, B. (2007). The depth distribution of azimuthal anisotropy in the continental upper mantle. *Nature*, *447*, 198–201. https://doi.org/10.1038/nature05742

Metcalfe, I. (2000). The Bentong-Raub Suture Zone. *Journal of Asian Earth Sciences*, *18*, 691–712. https://doi.org/10.1016/S1367-9120(00)00043-2

Metcalfe, I. (2013). Tectonic evolution of the Malay Peninsula. *Journal of Asian Earth Sciences*, *76*, 195–213. https://doi.org/10.1016/j.jseaes.2012.12.011

Morley, C. K. (2001). Combined escape tectonics and subduction rollback-back arc extension: A model for the evolution of Tertiary rift basins in Thailand, Malaysia and Laos. *Journal of the Geological Society*, *158*, 461–474. https://doi.org/10.1144/jgs.158.3.461

Pubellier, M., & Morley, C. K. (2014). The basins of Sundaland (SE Asia): Evolution and boundary conditions. *Marine and Petroleum Geology*, *58*, 555–578. https://doi.org/10.1016/j.marpetgeo.2013.11.019

Reed, C. A., Liu, K. H., Yu, Y., & Gao, S. S. (2017). Seismic anisotropy and mantle dynamics beneath the Malawi Rift Zone, East Africa. *Tectonics*, *36*, 1338–1351. https://doi.org/10.1002/2017TC004519

Refayee, H. A., Yang, B. B., Liu, K. H., & Gao, S. S. (2014). Mantle flow and lithosphere-asthenosphere coupling beneath the southwestern edge of the North American craton: Constrains from shear-wave splitting measurements. *Earth and Planetary Science Letters*, *402*, 209–220. https://doi.org/10.1016/j.epsl.2013.01.031

Savage, M. K. (1999). Seismic anisotropy and mantle deformation: What have we learned from shear wave splitting? *Reviews of Geophysics*, *37*, 65–106. https://doi.org/10.1029/98RG02075

Schellart, W. P., & Lister, G. S. (2005). The role of the East Asian active margin in widespread extensional and strike-slip deformation in East Asia. *Journal of the Geological Society*, *162*, 959–972. https://doi.org/10.1144/0016-764904-112

Shi, X., Kirby, J., Yu, C., Jiménez-Díaz, A., & Zhao, J. (2017). Spatial variations in the effective elastic thickness of the lithosphere in Southeast Asia. *Gondwana Research*, *42*, 49–62. https://doi.org/10.1016/j.gr.2016.10.005

Silver, P. G. (1996). Seismic anisotropy beneath the continents: Probing the depths of geology. *Annual Review of Earth and Planetary Sciences*, *24*, 385–432. https://doi.org/10.1146/annurev.earth.24.1.385

Silver, P. G., & Chan, W. W. (1991). Shear wave splitting and subcontinental mantle deformation. *Journal of Geophysical Research*, *96*, 16429–16454. https://doi.org/10.1029/91JB00899

Silver, P. G., & Savage, M. K. (1994). The interpretation of shear-wave splitting parameters in the presence of two anisotropic layers. *Geophysical Journal International*, *119*, 949–963. https://doi.org/10.1111/j.1365-246x.1994.tb04027.x

Simons, W. J. F., Socquet, A., Vigny, C., Ambrosius, B. A. C., Haji Abu, S., Promthong, C., et al. (2007). A decade of GPS in Southeast Asia: Resolving Sundaland motion and boundaries. *Journal of Geophysical Research*, *112*, B06420. https://doi.org/10.1029/2005JB003868

Song, W., Yu, Y., Shen, C., Lu, F., & Kong, F. (2019). Asthenospheric flow beneath the Carpathian-Pannonian region: Constraints from shear wave splitting analysis. *Earth and Planetary Science Letters*, *520*, 231–240. https://doi.org/10.1016/j.epsl.2019.05.045

Tang, Q., & Zheng, C. (2013). Crust and upper mantle structure and its tectonic implications in the South China Sea and adjacent regions. *Journal of Asian Earth Sciences*, *62*, 510–525. https://doi.org/10.1016/j.jseaes.2012.10.037

Wang, L., & He, X. (2020). Seismic anisotropy in the Java-Banda and Philippine subduction zones and its implications for the mantle flow system beneath the Sunda plate. *Geochemistry, Geophysics, Geosystems*, *21*, e2019GC008658. https://doi.org/10.1029/2019GC008658

Wessel, P., & Smith, W. H. F. (1998). New, improved version of generic mapping tools released. *Eos, Transactions American Geophysical Union*, *79*, 579. https://doi.org/10.1029/98EO00426

Whittaker, J. M., Müller, R. D., Sdrolias, M., & Heine, C. (2007). Sunda-Java trench kinematics, slab window formation and overriding plate deformation since the Cretaceous. *Earth and Planetary Science Letters*, *255*, 445–457. https://doi.org/10.1016/j.epsl.2006.12.031

Xue, M., Le, K. P., & Yang, T. (2013). Seismic anisotropy surrounding South China Sea and its geodynamic implications. *Marine Geophysical Research*, *34*, 407–429. https://doi.org/10.1007/s11001-013-9194-4

Yang, B., Liu, Y., Dahm, H., Liu, K. H., & Gao, S. S. (2017). Seismic azimuthal anisotropy beneath the eastern United States and its geodynamic implications. *Geophysical Research Letters*, *44*, 2670–2678. https://doi.org/10.1002/2016GL071227

Yu, C., Shi, X., Yang, X., Zhao, J., Chen, M., & Tang, Q. (2017). Deep thermal structure of Southeast Asia constrained by S-velocity data. *Marine Geophysical Research*, *38*, 341–355. https://doi.org/10.1007/s11001-017-9311-x

Yu, Y., Gao, S. S., Liu, K. H., Yang, T., Xue, M., Le, K. P., & Gao, J. (2018). Characteristics of the mantle flow system beneath the Indochina Peninsula revealed by teleseismic shear wave splitting analysis. *Geochemistry, Geophysics, Geosystems*, *19*, 1519–1532. https://doi.org/10.1029/2018GC007474

Yu, Y., Gao, S. S., Moidaki, M., Reed, C. A., & Liu, K. H. (2015). Seismic anisotropy beneath the incipient Okavango rift: Implications for rifting initiation. *Earth and Planetary Science Letters*, *430*, 1–8. https://doi.org/10.1016/j.epsl.2015.08.009

Yu, Y., Hung, T. D., Yang, T., Xue, M., Liu, K. H., & Gao, S. S. (2017). Lateral variations of crustal structure beneath the Indochina Peninsula. *Tectonophysics*, *712–713*, 193–199. https://doi.org/10.1016/j.tecto.2017.05.023

Zahirovic, S., Matthews, K. J., Flament, N., Müller, R. D., Hill, K. C., Seton, M., & Gurnis, M. (2016). Tectonic evolution and deep mantle structure of the eastern Tethys since the latest Jurassic. *Earth-Science Reviews*, *162*, 293–337. https://doi.org/10.1016/j.earscirev.2016.09.005

Zenonos, A., De Siena, L., Widiyantoro, S., & Rawlinson, N. (2019). P and S wave travel time tomography of the SE Asia-Australia collision zone. *Physics of the Earth and Planetary Interiors*, *293*, 106267. https://doi.org/10.1016/j.pepi.2019.05.010

Zhang, S., & Karato, S. (1995). Lattice preferred orientation of olivine aggregates deformed in simple shear. *Nature*, *375*, 774–777. https://doi.org/10.1038/375774a0